Role of transient water pressure in quarrying: A subglacial experiment using acoustic emissions

D. Cohen,[1] T. S. Hooyer,[2] N. R. Iverson,[1] J. F. Thomason,[1] and M. Jackson[3]

Received 10 November 2005; revised 13 March 2006; accepted 21 March 2006; published 5 August 2006.

[1] Probably the most important mechanism of glacial erosion is quarrying: the growth and coalescence of cracks in subglacial bedrock and dislodgement of resultant rock fragments. Although evidence indicates that erosion rates depend on sliding speed, rates of crack growth in bedrock may be enhanced by changing stresses on the bed caused by fluctuating basal water pressure in zones of ice-bed separation. To study quarrying in real time, a granite step, 12 cm high with a crack in its stoss surface, was installed at the bed of Engabreen, Norway. Acoustic emission sensors monitored crack growth events in the step as ice slid over it. Vertical stresses, water pressure, and cavity height in the lee of the step were also measured. Water was pumped to the lee of the step several times over 8 days. Pumping initially caused opening of a leeward cavity, which then closed after pumping was stopped and water pressure decreased. During cavity closure, acoustic emissions emanating mostly from the vicinity of the base of the crack in the step increased dramatically. With repeated pump tests this crack grew with time until the step's lee surface was quarried. Our experiments indicate that fluctuating water pressure caused stress thresholds required for crack growth to be exceeded. Natural basal water pressure fluctuations should also concentrate stresses on rock steps, increasing rates of crack growth. Stress changes on the bed due to water pressure fluctuations will increase in magnitude and duration with cavity size, which may help explain the effect of sliding speed on erosion rates.

Citation: Cohen, D., T. S. Hooyer, N. R. Iverson, J. F. Thomason, and M. Jackson (2006), Role of transient water pressure in quarrying: A subglacial experiment using acoustic emissions, *J. Geophys. Res.*, *111*, F03006, doi:10.1029/2005JF000439.

1. Introduction

[2] Glacial erosion plays a major role in sediment production and the evolution of glaciated landscapes. Over the last two decades, this process has received considerable attention because of its likely effect on uplift in orogenic belts, weathering rates and atmospheric CO_2, and related past changes in global climate [e.g., *Molnar and England*, 1990; *Raymo and Ruddiman*, 1992; *Hallet et al.*, 1996; *Brocklehurst and Whipple*, 2002; *Jaeger et al.*, 2001; *Tomkin*, 2003; *Spotila et al.*, 2004]. Central to large-scale models for estimating patterns and rates of glacial erosion is the rule that links glaciological variables to the bedrock erosion rate.

[3] This rule is poorly known. Most models of glacial erosion assume that either ice discharge [*Anderson et al.*, 2006] or more specifically sliding speed is the dominant control on bedrock erosion rate [e.g., *Harbor*, 1992; *Braun et al.*, 1999; *MacGregor et al.*, 2000; *Tomkin*, 2003]. Measurements of sediment discharge over seasonal timescales in outlet streams [*Humphrey and Raymond*, 1994; *Riihimaki et al.*, 2005] indicate that erosion rates are correlated to sliding speed. However, interpretations are not straightforward owing to potential storage of debris under or within basal ice that may be released as ice-bed separation increases with increasing sliding velocity. In contrast, others have argued that bedrock erosion rate depends primarily on basal water discharge [*Alley*, 1999; *Alley et al.*, 1999], which determines the extent of basal water pressure variability. In this case, the modeling strategy is fundamentally different: water discharge is estimated to make model predictions with no attention paid to ice discharge or sliding velocity [*Alley et al.*, 1999].

[4] Simple parameterizations for large-scale models of glacial erosion are grounded on knowledge of erosional processes. Subglacial erosion of bedrock by water, although important locally, is thought to be volumetrically subordinate to abrasion and quarrying [e.g., *Drewry*, 1986]. Abrasion is relatively well understood: the wear law used in abrasion models [*Boulton*, 1974; *Hallet*, 1979; *Drewry*, 1986] has long been established in materials science [*Archad*, 1953] and subsequently tested in geophysical applications [*Scholz*, 1987]. There is also strong justification for assuming abrasion rate to increase with sliding velocity, which influences both the flux of abrasive particles

[1]Department of Geological and Atmospheric Sciences, Iowa State University, Ames, Iowa, USA.
[2]Wisconsin Geological and Natural History Survey, Madison, Wisconsin, USA.
[3]Norwegian Water Resources and Energy Directorate, Oslo, Norway.

0148-0227/06/2005JF000439

across the bed [*Boulton*, 1974; *Hallet*, 1979] and the force with which particles are pressed against stoss surfaces by sliding ice [*Hallet*, 1979; *Iverson*, 1990]. Most authors, however, consider quarrying to be more important than abrasion [*Jahns*, 1943; *Boulton et al.*, 1979; *Drewry*, 1986; *Iverson*, 2002], and this claim is supported by measurements [e.g., *Loso et al.*, 2004; *Riihimaki et al.*, 2005] and modeling [*Hildes et al.*, 2004].

[5] Quarrying is thought to be rate limited by crack growth and not by entrainment of fractured bedrock [e.g., *Hallet*, 1996]. Static deviatoric stresses in rock beneath glaciers are too small to fracture flawless bedrock but are sufficiently large to cause subcritical growth of preexisting cracks: slow, stable crack growth due mainly to stress-corrosion reactions that cause weakening of atomic bonds at crack tips [*Atkinson*, 1984]. In this regime, a mode I (extensional) crack will grow if the tensile stress near its tip exceeds the stress-corrosion limit. Linear elasticity theory provides a method for estimating the near-tip stress field by relating it to the remote applied stress through the stress intensity factor. For example, for a two-dimensional, internal crack that is penny shaped and perpendicular to a far field tension T, the near-tip tension σ and stress intensity factor K_I (subscript I refers to mode I cracks) are given by [*Lawn and Wilshaw*, 1975]

$$\sigma = \frac{K_I}{\sqrt{2\pi r}}, \tag{1}$$

$$K_I = Y T \sqrt{\pi a}, \tag{2}$$

where r is the distance from the crack tip, Y is a dimensionless parameter that depends on both specimen and crack geometries, and a is half the length of the crack. The rate of subcritical crack growth, v, is a highly nonlinear function of the stress intensity factor [*Atkinson*, 1984]. An empirical equation used commonly to describe v is *Charles*'s [1958] law:

$$v = v_o \exp\left(\frac{-H}{RT}\right) K_I^m, \tag{3}$$

where H is the activation enthalpy, R is the gas constant, T is the temperature, and v_o and m are material constants determined from experiments. The value of m can be as high as 50 for rocks [e.g., *Atkinson*, 1984]. The stress enhancement at crack tips (given by K_I) in excess of the stress-corrosion limit may enable slow crack growth under relatively small stress differences in the bed.

[6] Unlike abrasion rate, which clearly depends on sliding speed, the dominant glaciological variable that affects quarrying rate is not clear. Quantitative analyses of quarrying [*Iverson*, 1991; *Hallet*, 1996] emphasize the role of ice-bed separation in promoting crack growth in the bed. As cavities grow down glacier from steps or bumps on the bed, areas of ice-bed contact diminish, increasing normal stresses on those areas and thereby promoting crack growth in the bed. Cavity size increases with sliding velocity and depends inversely on effective pressure, the difference between the ice overburden pressure and cavity water pressure.

[7] Quarrying may be enhanced by fluctuations in basal water pressure [*Iverson*, 1991]. Water pressure in basal cavities varies as a function of surface water input to the bed (see review by *Fountain and Walder* [1998]). Conditions for crack growth in the bed should be optimized by water pressure decreases in lee-side cavities. During and potentially after reductions in water pressure, deviatoric stresses in the bed can exceed those with a steady state cavity, because water pressure can decrease at a rate faster than the rate of cavity closure, temporarily resulting in large cavities under low water pressure, the optimum situation for large stress differences in the bed. Thus rates of quarrying may depend on the time derivative of water pressure, such that the frequency and amplitude of water pressure fluctuations strongly influence quarrying rate.

[8] We have attempted to test this hypothesis in an experiment beneath Engabreen, an outlet glacier of the Svartisen Ice Cap in northern Norway. Access to the bed there beneath 213 m of sliding, temperate ice is provided by tunnels through the rock bed. An instrumented panel containing a 12 cm high granite rock step was installed beneath the glacier using the same system for accessing the bed as in earlier experiments [*Cohen et al.*, 2000, 2005; *Iverson et al.*, 2003]. Water was pumped to the bed, increasing the water pressure and inducing a cavity in the lee of the step. We monitored crack growth activity and location by recording high-frequency elastic waves (acoustic emissions) emitted by propagating cracks. These measurements demonstrate that a preexisting crack in the step grew rapidly in response to water pressure decreases until a rock fragment was eventually quarried.

2. Field Setting

[9] Housed inside a rock tunnel beneath Engabreen, the Svartisen Subglacial Laboratory provides access to the glacier bed through a 5 m high vertical shaft. This shaft opens onto the bed through a 0.60 m square hole beneath 213 m of ice. To prevent ice from entering the shaft, a flat steel plate, supported underneath by a scaffold, seals the hole. The scaffold consists of a table on top of removable legs that extend to the floor of the tunnel. Winching cables allow lowering of the table and the steel plate, which can then be loaded with a panel containing instruments. When the panel is winched upward into position, its upper surface is in direct contact with basal ice sliding at $\sim$0.12 m d^{-1} [*Cohen et al.*, 2000] (Figure 1).

[10] Gneissic bedrock with meter to decameter-scale undulations underlies the glacier. Tunnels melted along the bed in early spring during past field seasons [*Cohen et al.*, 2000; *Iverson et al.*, 2003] indicate that ice is typically in direct contact with rock with no intervening till and that cavities are not usually present on lee surfaces of bedrock highs, probably because water is in limited supply then. Thus to study the effect of water pressure variability on quarrying, water must be pumped to the glacier bed to manipulate water pressure and form basal cavities. Subglacial experiments cannot be conducted safely later, during

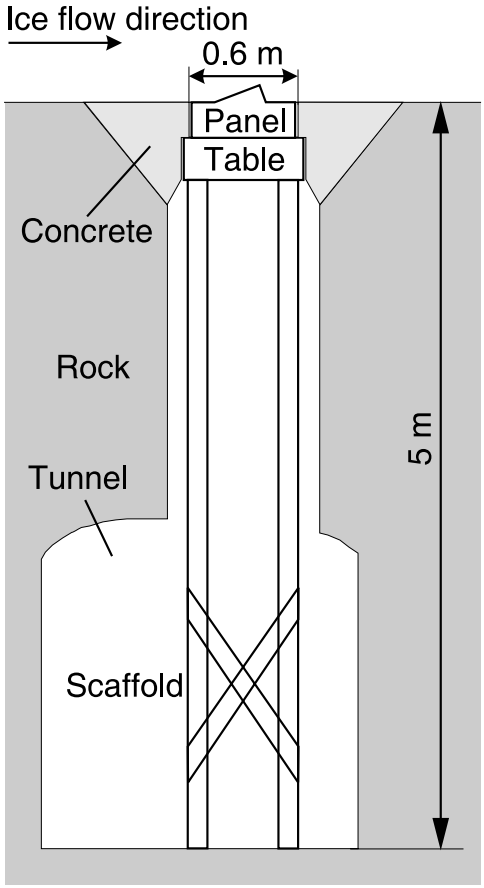

Figure 1. Cross section of tunnel and vertical shaft showing panel, supporting table, and scaffold.

the melt season, owing to sporadic flooding of the tunnel system.

3. Apparatus

[11] The apparatus for this experiment had two parts: a panel containing the rock step and transducers and an acoustic emission data acquisition system located in the underlying tunnel.

3.1. Instrumented Panel

[12] A panel (Figures 2 and 3), 58 cm square and 20 cm high, constructed from aluminum plates, contained at its center a granite step, of which 12 cm protruded above the surrounding panel into the basal ice. The step's shape and dimensions were chosen on the basis of constraints imposed by the size of the panel. The step, 37 cm long and 25 cm wide, was oriented within the panel (Figure 2a) so that the lip of the step was perpendicular to the ice flow direction known from striations on a flat rock tablet installed at the top of the vertical shaft during an earlier experiment [*Cohen et al.*, 2005]. The up-glacier face of the step was inclined at an angle of 20° from the flat upper surface of the panel and met the down-glacier face at a right angle (Figure 2b). The step, sawed from Chelmsford granite (Fletcher Co. of North Chelmsford, Mass.), was cut such that the orientations of the rift and grain planes [see *Peng and Johnson*, 1972] were parallel to the down-glacier and up-glacier faces of the step, respectively. The rift plane is the plane of easiest splitting. Chelmsford granite was selected because it is easily available and has a small fracture toughness relative to other granites, so it fractures more readily. Marble or sandstone, although weaker than granite and thus likely easier to quarry, tends to have greater anisotropy [see *Atkinson*, 1984, Table 2], which complicates interpretation of acoustic emissions.

[13] To help ensure quarrying and provide a well-defined locus for crack growth at a known location, a crack, 2 mm wide and 31 mm deep, was cut 31 mm up-glacier from the lip of the step and normal to the stoss surface (Figure 2b). The granite step was epoxied inside a steel carriage made with a 19.0 mm thick bottom plate. The bottom plate rested on another 19.0 mm thick steel plate with lubricant between them. The lubricant, a mixture of 80% Vaseline and 20% stearic acid [*Labuz and Bridell*, 1993], had a low friction coefficient [*Cohen et al.*, 2000] that minimized horizontal friction between the carriage and the underlying steel plate. Minimizing friction was essential for the correct operation of an underlying 1 MN annular load cell (Geokon, model 4900X-225000-8.843), 22.46 cm in diameter, that recorded the vertical ice load on the step (Figures 2a and 2b). Screws with their tips lubricated to minimize vertical friction allowed centering of the carriage inside the aluminum frame of the panel. The gap between the carriage and the frame was less than 1 mm. During the experiment, the gap filled with fine sediments that helped prevent escape of water from the bed through the panel. The gap between the panel and the shaft opening was sealed with a strip of rubber gasket at the perimeter of the base of the panel. Once the panel was in position at the top of the shaft, the gasket was compressed between the table beneath the panel and the concrete near the top of the vertical shaft (Figure 2b).

[14] Two load cells (Geokon, model 4900X-10-0), one upstream of the step and one downstream (Figure 2a), recorded the vertical stress exerted by the ice away from the step. Each load cell was supported below by an aluminum block screwed into the sides of the panel. Disks, 50 mm in diameter and flush with the upper surface of the panel, pressed on top of the load cells and isolated the sensors from the ice. Each load cell recorded a force normal to the bed over a 16 cm^2 footprint. Two water pressure transducers (Geokon, model 4500SH-500), enclosed in sealed aluminum cylinders attached to the bottom of the panel's cover plate, measured the water pressure at the glacier bed through 5 mm diameter ports. Porous ceramic tips (50 kPa air entry pressure) screened the ports at their tops. The ports were filled with water before the experiment to expel air bubbles. A 10 MPa, 6 L min^{-1}, high-pressure pump (Kärcher, model 5.20M) was connected through a hose to an orifice just downstream of the step to manipulate the basal water pressure (Figure 2a).

[15] Attempts were made to measure sliding speed and cavity size with variable success. As in earlier experiments [e.g., *Cohen et al.*, 2005], we attempted to record sliding speed with a plastic ball (Figure 3) attached to a stainless steel cable that passed through a sealed hole in the panel's cover plate. When this device works properly, the ball is entrained in basal ice and the cable is withdrawn from the panel during glacier slip at a rate recorded by an extensometer (Unim-

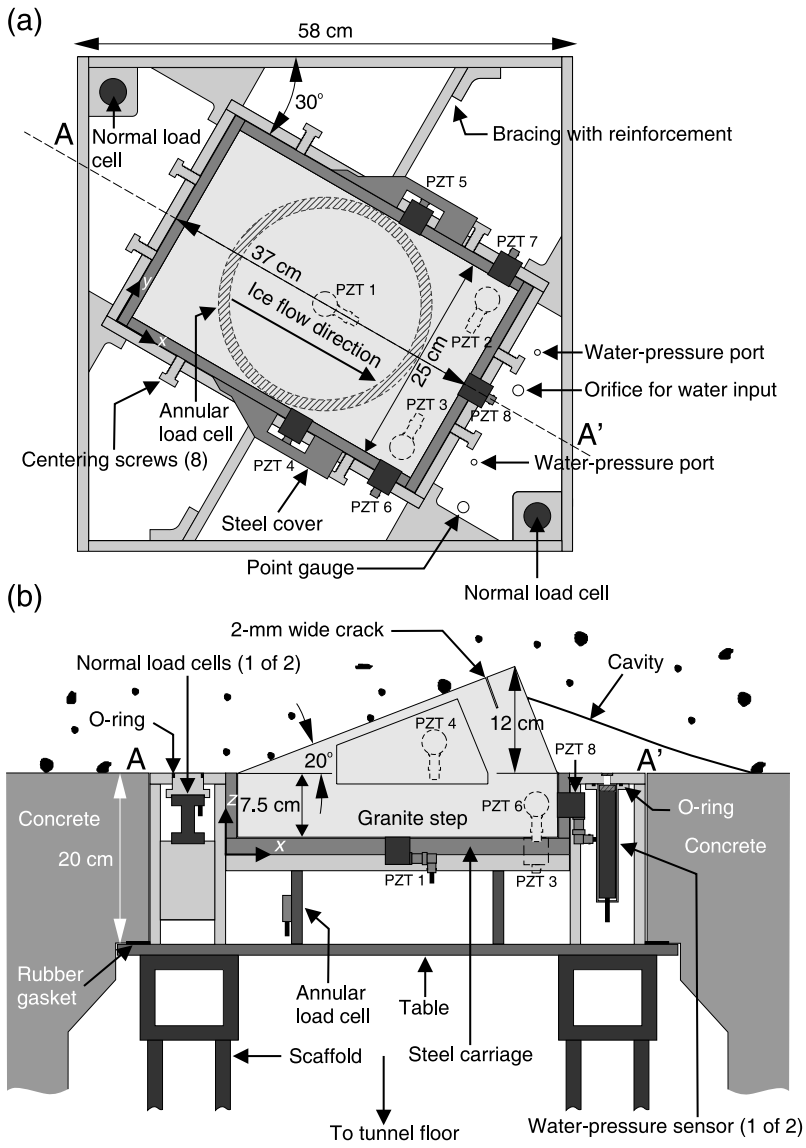

Figure 2. (a) Top view showing inside and (b) cross-section AA′ of panel. Some components are shown that are outside the AA′ plane. See main text for description of AE sensor locations.

easure, model HX-PA-60) in the tunnel. In addition, cavity height near the edge of the step was measured 12 cm downstream from the step's lip with a point gauge (Figure 2a). This gauge consisted of a steel rod that could be slid through the panel's upper surface until it was in contact with the cavity ceiling. This rod was sealed with an O-ring and could be operated from beneath the panel.

3.2. Acoustic Emission Monitoring System

[16] Crack propagation was monitored using an acoustic emission (AE) data acquisition system that permits continuous measurement of crack activity and location. Acoustic emissions are high-frequency, short-lived, elastic waves generated by rapid release of stored elastic strain energy from a localized source [*Lockner*, 1993]. In crystalline rocks, dislocations, grain boundary movements, twinning, and growth of fractures through or between mineral grains cause acoustic emissions [e.g., *Lavrov and Shkuratnik*, 2005]. The AE waveform is transformed through wave propagation, sensor response, and signal acquisition, so the observed signal bears little resemblance to the original waveform. Detection of signals above a threshold voltage, counting these emissions, and locating their sources are the simplest processing steps for characterizing AE activity [*Lockner*, 1993]. More complicated signal processing, such as moment tensor analysis, has been used to determine crack growth modes and event location in laboratory and in situ settings [e.g., *Shah and Labuz*, 1995; *Chang and Lee*, 2004]. In our experiments we focused on signal detection, emission counts, and event locations.

[17] Eight piezoelectric transducers (Physical Acoustic Corporation, model R151-AST), 21 mm in diameter, with integral 40 dB gain preamplifiers to remove low-frequency noise, were coupled to the surface of the granite step with silicone vacuum grease (PZT 1 through 8, Figure 2). Screws pressed lightly on padded metal disks in contact with the back of transducers to hold them firmly to the rock surface. These broadband transducers had highest sensitivities in the

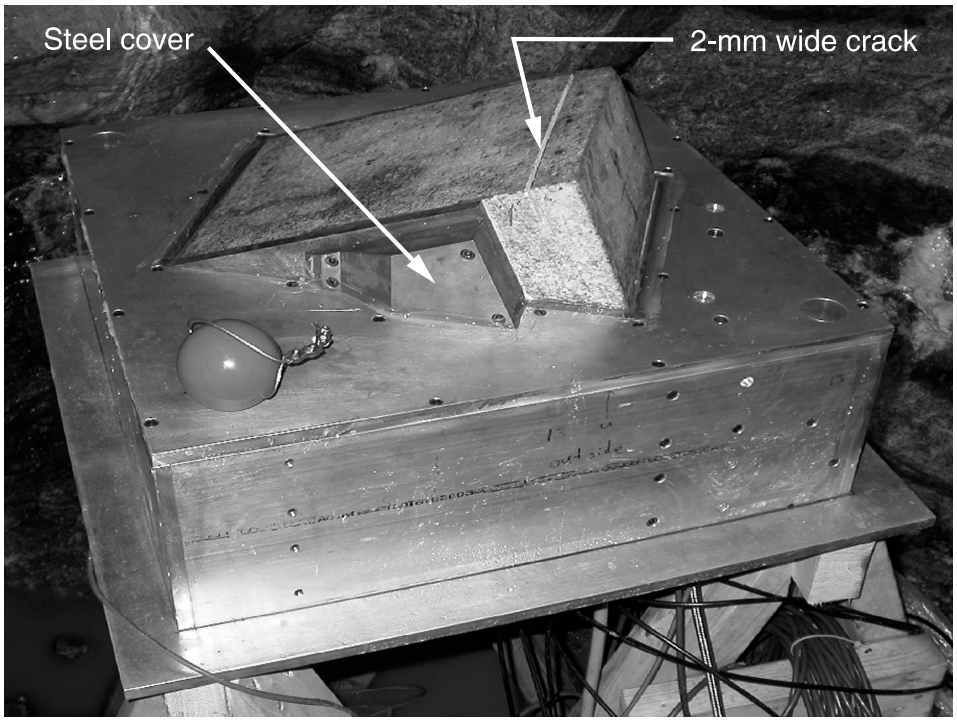

Figure 3. Panel on table at the bottom of the vertical shaft. Sphere at bottom left corner of panel was the anchor for measuring sliding velocity.

frequency range between 70 and 200 kHz with a resonant frequency of 150 kHz. Three transducers (PZT 1–3) were positioned to form a triangle at the bottom of the granite block. Another transducer (PZT 8) was centered on the down-glacier side of the step below the panel's upper surface. Four more transducers (PZT 4–7), two on each side of the rock step, were positioned so that one on each side was above the top surface of the panel (PZT 4 and 5). Transducers above the panel's upper surface were protected from the ice by steel covers (Figure 3). This configuration optimized locating AE events.

[18] An acoustic emission data acquisition system (Samos, Physical Acoustic Corporation) consisting of a desktop computer with an 8 channel, 16 bit, 1 MHz A/D converter was installed in the tunnel system in a sealed enclosure kept at a constant temperature of 15°C by a small electric heater. Cables running from the AE sensors to the data acquisition system were 10 m long. Owing to internal preamplifiers in the AE sensors, loss of signal over the length of the cable was negligible. The system was triggered by the arrival of an AE signal exceeding a fixed threshold voltage set at 45 dB (178 μV). AE activity was monitored at each transducer by tracking the number of threshold crossings (hits) and the time of arrival of the first hit at each transducer. Other AE characteristics were also collected, but in most cases only the number of hits and first arrival times were used for determining AE frequency and event location. Absolute time resolution was 0.25 μs.

4. Procedures

4.1. Location of AE Events

[19] In theory, the location of an AE event in three dimensions can be obtained with only four transducers if the difference in arrival time of the AE wave is precisely known between transducers and the wave velocity is known, constant, and isotropic. In practice, additional transducers are useful to reduce errors. In the present study we used all eight transducers to determine the location of an AE event, which was computed with data acquisition software provided by Physical Acoustic Corporation. The method minimizes the function $\mathcal{F}$,

$$\mathcal{F} = \sum_{i=1, i\neq f}^{N_t} \left(\Delta T_i^{obs} - \Delta T_i^{calc}\right), \tag{4}$$

$$\Delta T_i^{calc} = \frac{\|\mathbf{x}_i - \mathbf{x}_f\|}{s}, \tag{5}$$

where N_t is the number of transducers (the summation excludes the first hit transducer, f), ΔT_i^{obs} is the observed difference in arrival time between transducer i and the first hit transducer, ΔT_i^{calc} is the calculated difference in arrival time for the same two transducers, $\mathbf{x}_i$ and $\mathbf{x}_f$ are the three-dimensional coordinates of the ith and f transducers, and s is the wave speed. The minimization is performed by searching across the three-dimensional space using the simplex method [*Nelder and Mead*, 1965].

[20] The wave speed, s, was measured in the rock step prior to the field experiment. Using one AE sensor as a pulse generator, the time for the wave to travel through the rock step and reach other AE sensors was measured and the wave speed determined. The average wave speed was 4 ± 1 km s^{-1}. A more precise value could not be obtained because of finite transducer contact area and wave speed anisotropy due to rock heterogeneity. Given

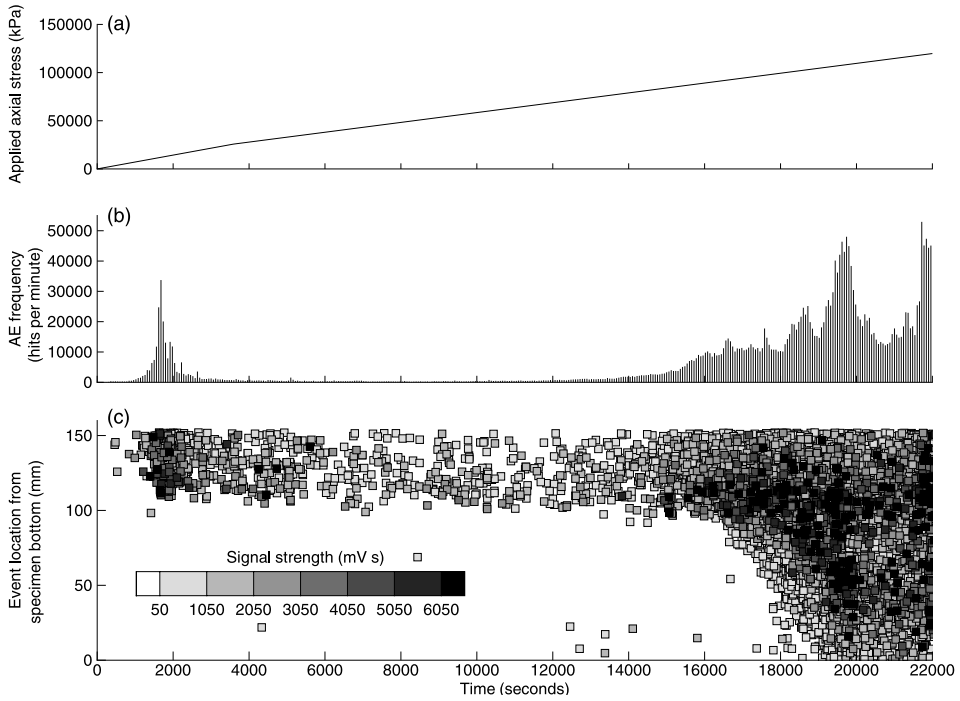

Figure 4. Laboratory results showing (a) applied axial stress, (b) AE frequency, and (c) locations of AE events as a function of time. Events in (c) are shaded according to the strength of the voltage signal calculated as the integral of the voltage over the duration of the AE event.

the 0.25 μs time resolution of the AE system, the spatial resolution was 1 mm.

[21] The event location method was tested by breaking pencil leads at known positions on the surface of the rock step (lead pencil break tests are also known as Hsu-Nielsen sources [*Breckenridge et al.*, 1990]). In general, the three-dimensional coordinates of an event could be determined to within only about 20 mm, owing to finite transducer contact area and small distances between sensors. For lead pencil break tests conducted near expected AE sources in the field experiments (i.e., near the tip of the crack), the vertical coordinate of an AE event could be determined to within 10 mm.

[22] Another test of the location method was provided by loading progressively a rectangular sample of Chelmsford granite (76 × 76 × 152 mm) in a servo-controlled hydraulic press (Satec System Inc., model MII400RD) while monitoring AE activity. The specimen was loaded parallel to its long axis (perpendicular to the hardway plane [*Peng and Johnson*, 1972]) until failure occurred. The ends in contact with the press were lubricated with a mixture of stearic acid and Vaseline [*Labuz and Bridell*, 1993] to reduce friction at the interfaces and thus obtain a more uniform state of stress. A 3-mm wide, 19-mm deep crack parallel to the rift plane was cut at the top of the specimen across its entire width to reduce the compressive strength of the rock and to serve as a locus for crack propagation. Eight AE transducers, two on each of the four rectangular faces, were placed at heights 25 and 121 mm, respectively, from the bottom of the specimen to record AE activity as the specimen was loaded. The loading rate was 2.2 kN min^{-1} until a load of 133 kN was reached; the loading rate was then decreased to 1.78 kN min^{-1} until failure occurred.

[23] Soon after the beginning of the test (1800 s), AE activity increased: uneven loading of the top surface of the block (which was not cut with machine precision) presumably caused microcracking in the upper 40 mm of the block resulting in a burst of high-strength AE events (Figure 4). Thereafter, AE activity remained low with only a few events of low strength concentrated in the upper 50 mm of the block. Starting at 12,000 s, AE activity increased in several steps, progressively at first and then more rapidly before a plateau. This was then followed by two large peaks of activity, with the latter leading to the shattering of the specimen. These stages of activity probably coincided with periods of crack initiation, crack coalescence, and crack propagation largely parallel to the most compressive stress [e.g., *Brace*, 1964; *Bieniawski*, 1967; *Eberhardt et al.*, 1999].

[24] During periods of elevated AE activity, events became more energetic (higher signal strength). More importantly, AE source locations spread down the vertical axis of the block (Figure 4c) eventually occurring over the entire specimen before failure (22,000 s). Analysis of the rock specimen indicated that failure occurred along several vertical planes parallel to the weak rift plane. One of these planes initiated at the base of the preexisting crack. Although AE events could not be correlated to a particular crack, these tests showed that spatial migration of events caused by crack propagation could be detected and used to calculate crack growth rates.

4.2. Field Experiment

[25] To install the panel, a small cavity was made in the ice above the vertical shaft to allow the protruding rock step to fit at the top of the scaffold (Figure 1). Once the panel was in place, load cells for measuring vertical stresses and

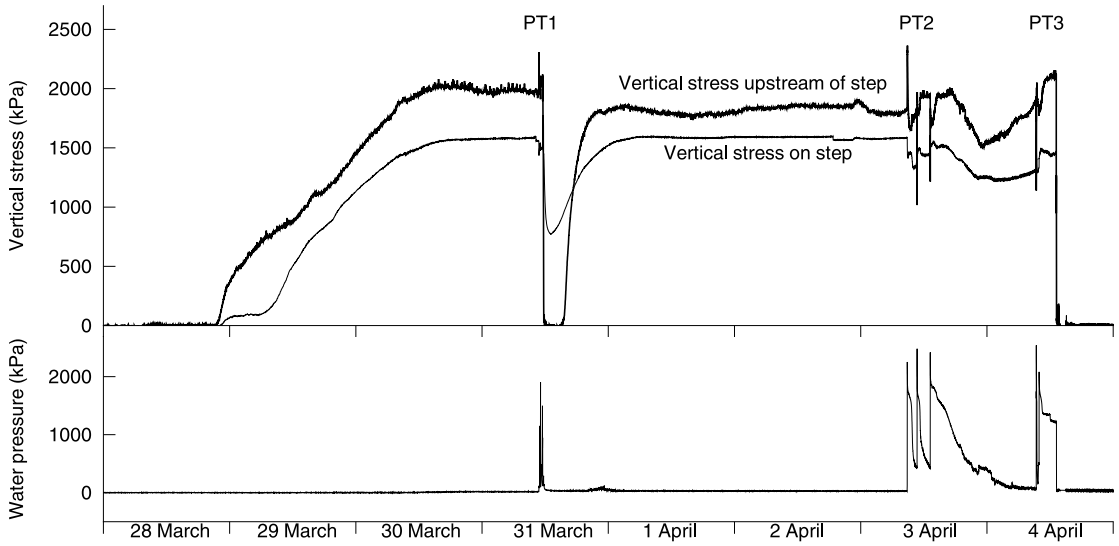

Figure 5. Time series of mean vertical stress on the step, the local stress on the bed upstream, and average water pressure. PT1, PT2, and PT3 indicate the timing of the pump tests.

water pressure sensors were connected to a Campbell CR10X data logger located in the tunnel. Data were collected every 15 s to 1 min. AE sensors recorded continuously. After normal stresses reached steady values, pump tests were initiated. Each test consisted of pumping water (at about 2°C) to the lee of the rock step to open a cavity. Monitoring of the height of the cavity and of normal stresses was used to determine when pumping was stopped. Water pressure was then allowed to fall and the cavity to close until steady state conditions prevailed before starting a new pump test. At the end of the pumping experiments, the panel was lowered and the rock step was examined.

5. Results

[26] The panel was installed at the top of the vertical shaft on 27 March 2004. Figure 5 shows the mean vertical stress on the step averaged over its full area (stoss and lee surface), the stress on the bed upstream averaged over a small load cell platen, and the average water pressure during the experiment, which included three pump tests (PT1 through PT3). The signal of the downstream load cell is not shown because of calibration problems. Its signal mimicked the water pressure record during the pump tests but was offset by about 600–1000 kPa. In addition, the cable linking the ball to the extensometer was severed early in the experiment, so a record of sliding speed was not obtained. After several days of transient adjustments as ice closed on the rock step (28 March to 30 March), values of stresses became steady (Figure 5). Water pressure remained close to zero because a seal had not yet been achieved between the basal hydraulic system and the tunnel. Downward stress on the flat portion of the panel upstream of the step indicated values around 1950 kPa while the mean vertical stress on the rock step was smaller (1650 kPa).

[27] Pumping of water under high pressure during the first pump test (PT1, Figure 6a) caused water to leak into the tunnel through the gap between the panel and the shaft. Water pressure, measured in the lee of the step, was erratic and never reached a value higher than 2000 kPa except for a few tens of seconds. The point gauge indicated that a cavity grew in response to the pumping. About 1 hour into the pump test (1145), downward stress upstream of the rock step decreased abruptly to zero, and the mean vertical downward stress on the step began to decrease. The pump was then turned off (1200). The rate of decrease in mean stress on the step immediately began to decline. A minimum value of about half the ambient value before pumping was attained 1 hour later, and then the mean stress on the step began slowly increasing over ~12 hours back toward its ambient value. The record of the upstream load cell indicated no stress for about 3.5 hours after the pump was turned off (between 1200 and 1530), but stress increased rapidly thereafter. Before the pump test, AE frequency was small (100–200 hits per minute) but high during pumping (>2500 hits per minute). After the pump was turned off (1200), AE frequency remained steady at 300–400 hits per minute. During reloading of the step, AE frequency increased by a factor of 3–4, peaking at 1630 when both the mean stress on the step and vertical stress upstream of the step were increasing. As the loading rate on the step and on the load cell upstream decreased, AE activity diminished gradually to values observed before the pump test. The system was then allowed to equilibrate for 48 hours before the second pump test.

[28] During the second pump test (PT2, Figure 6b), water did not leak into the shaft. Upon turning on the pump (PT2a), basal water pressure rose in <30 seconds to the maximum pump pressure (10 MPa), causing the pump to automatically shut off. Water pressure then decayed in two discrete diffusive phases. The pump was then turned on again (PT2b), and as in PT2a, water pressure immediately peaked, and the pump shut off with a two-phase decay in water pressure. In contrast, during the third phase of pumping (PT2c), the pump did not shut off, and water was pumped for about 1 hour with only a slight decrease in water pressure. Water pressure decreased only slightly more rapidly after the pump was turned off (1426). Although

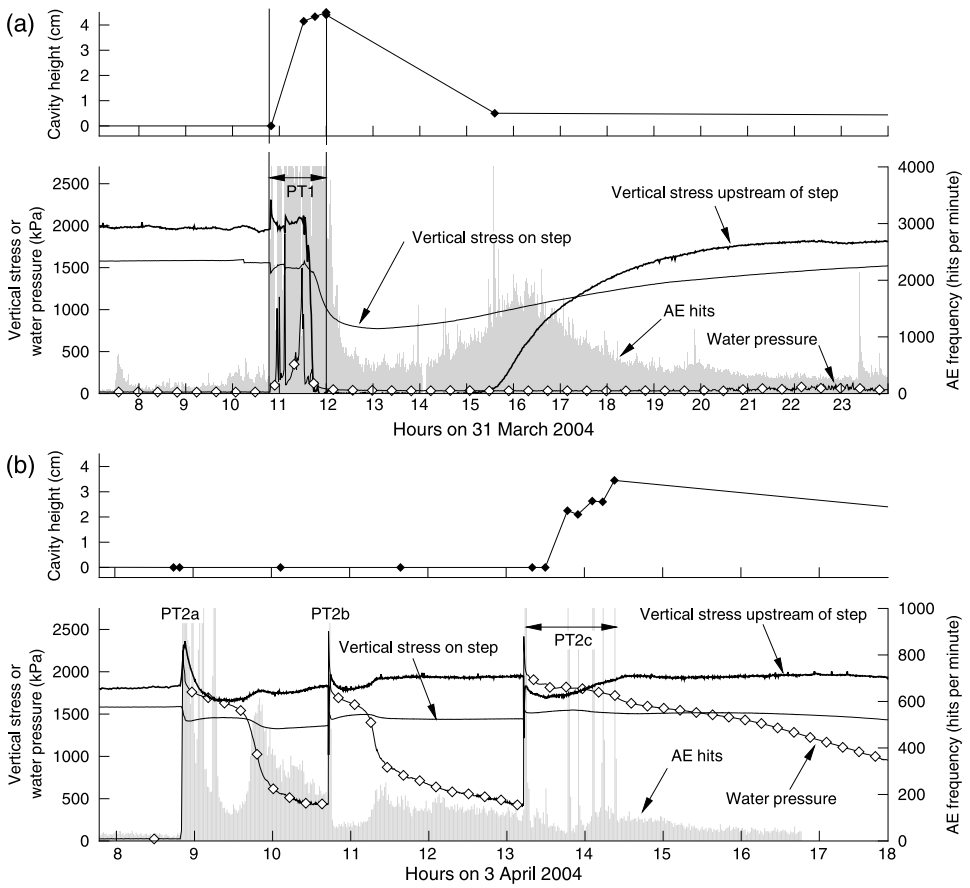

Figure 6. Cavity height, vertical stresses, average water pressure, and AE frequency during (a) pump test 1 (PT1), and (b) pump test 2 (PT2). Duration of pumping is indicated by horizontal, two-headed arrows for PT1 and PT2c. Pumping tests PT2a and PT2b lasted less than 1 min. AE activity is high during pumping because of panel vibrations.

stresses on the step and upstream of it underwent brief transient variations immediately during and after pumping, these variations were small relative to those of PT1. Most notable of these small variations was a peak in stress on the panel upstream of the step that followed the water pressure pulse by 4 minutes in PT2a and 1 min 30 s in PT2b. No ice-bed separation could be detected with the point gauge until 35 min into PT2c. As in PT1, AE frequency peaked markedly after pumping was stopped in PT2a and PT2b, although the time lag between the end of pumping and the peak AE frequency was about one quarter (~60 minutes) the time lag in PT1. No such peak in AE frequency occurred after pumping in PT2c.

[29] At 1645 on 3 April the AE data acquisition system quit working (Figure 6b) because of an electrical breakdown in the tunnel. The system was still not working during PT3, so that test is not considered further here.

[30] Time series of AE activity and effective pressure on the step (mean vertical stress on the step minus water pressure) for PT1, PT2a, and PT2b are shown in Figures 7a–7c, with corresponding plots of AE activity as a function of the time derivative of effective pressure (Figures 7d–7f). AE activity during pumping was neglected because panel vibrations were both visible and audible as water was forcibly injected to the glacier sole. Data from PT2c are not shown because there was no peak in AE activity after pumping.

[31] Figure 8 shows the locations of AE events projected onto the plane parallel to the ice flow direction. During PT1 (31 March, day 91, Figure 8a) most events were scattered in a zone centered around the tip of the preexisting crack but also near the base of the step. Fewer AE events were detected between the two pump tests (1–3 April, days 92–94, Figure 8b), whereas during PT2a,b (3 April, day 94, Figure 8c) many events were clustered farther down, closer to the base of the step's lee surface and none were apparent higher up. Few AE events were associated with PT2c (not shown in Figure 8).

[32] At the end of the tests on 4 April the panel was lowered, revealing a quarried surface that extended from the tip of the initial crack to the base of the lee surface (Figure 9). A rate of crack growth can be estimated for the period spanning PT1 and PT2 from the length of the crack (0.16 m) measured after the panel was lowered: 1.4×10^{-7} m s^{-1}. This value is within the range measured for other granitic rocks in laboratory tests [*Atkinson*, 1984]. Linear regressions of the vertical position of events that generated signal strength >5 mV s yield rough estimates of rates of crack growth during periods of enhanced AE activity (after PT1, PT2a, and PT2b) and during the quiescent period

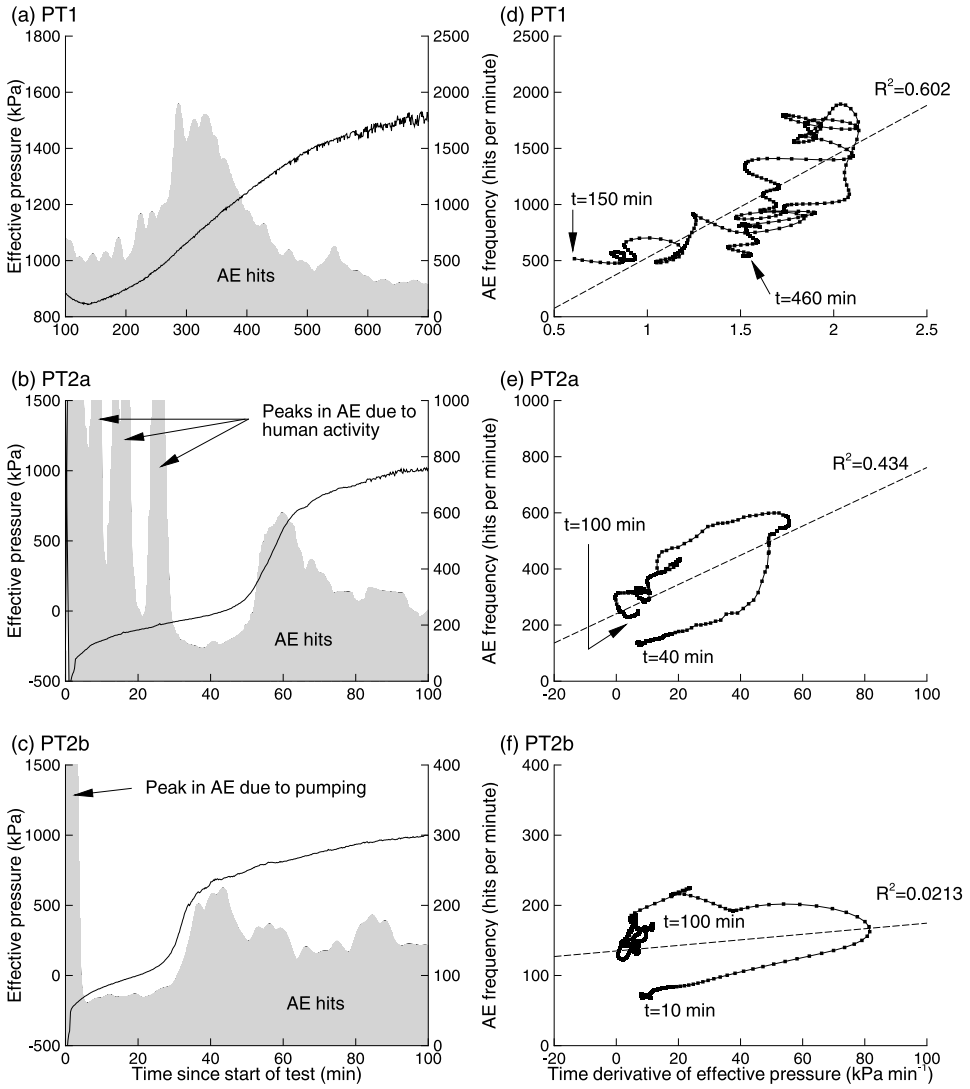

Figure 7. Effective stress and AE frequency as a function of time for (a) PT1, (b) PT2a, and (c) PT2b; corresponding plots of AE frequency as a function of the time derivative of the effective pressure for (d) PT1, (e) PT2a, and (f) PT2b. AE frequency and effective pressure were smoothed with a Laplacian algorithm to reduce high-frequency variations. In Figures 7d–7f, t is time since start of pump test. Dashed lines indicate linear best fits. R is the coefficient of linear regression.

between PT1 and PT2a: 8×10^{-7} m s^{-1} and 10^{-8} m s^{-1}, respectively. These numbers, however, are uncertain because of the scattering of the vertical position of events with time.

6. Discussion

6.1. Stress and Water Pressure Records

[33] Prior to the pumping experiments but after ice had closed on the panel, the mean stress on the step was significantly lower (1650 kPa) than the downward stress measured upstream of the panel (~1950 kPa). This difference may be due to vertical friction between centering screws (see Figure 2a) and the steel carriage containing the rock step. Despite uneven bed topography near the step, downward stress upstream of the panel was commensurate with the known ice thickness of 213 m (1916 kPa assuming an ice density of 917 kg m^{-3}).

[34] The records of stress and water pressure reveal changes in stress distribution and ice-bed separation associated with the pumping experiments. The largest changes were associated with PT1 (Figure 6a). Pumping of water to the lee of the step caused a cavity to grow, presumably due primarily to melting of ice. Water escaped through and around the panel and into the shaft. The abrupt reduction in stress on the bed upstream from the step after about 45 minutes of pumping indicated that ice had separated from the bed there. The reduction in downward stress on the step that began at about that time likely reflected loss of contact between some of the step's stoss surface and the ice, such that the force on the step fell slowly as the step was progressively exposed by melting. The mean stress on the step eventually decreased to about 50% of its ambient value, indicating that considerable but not total separation of ice from the step occurred. Figure 10a illustrates the likely shape of the cavity at the end of pumping. One hour after

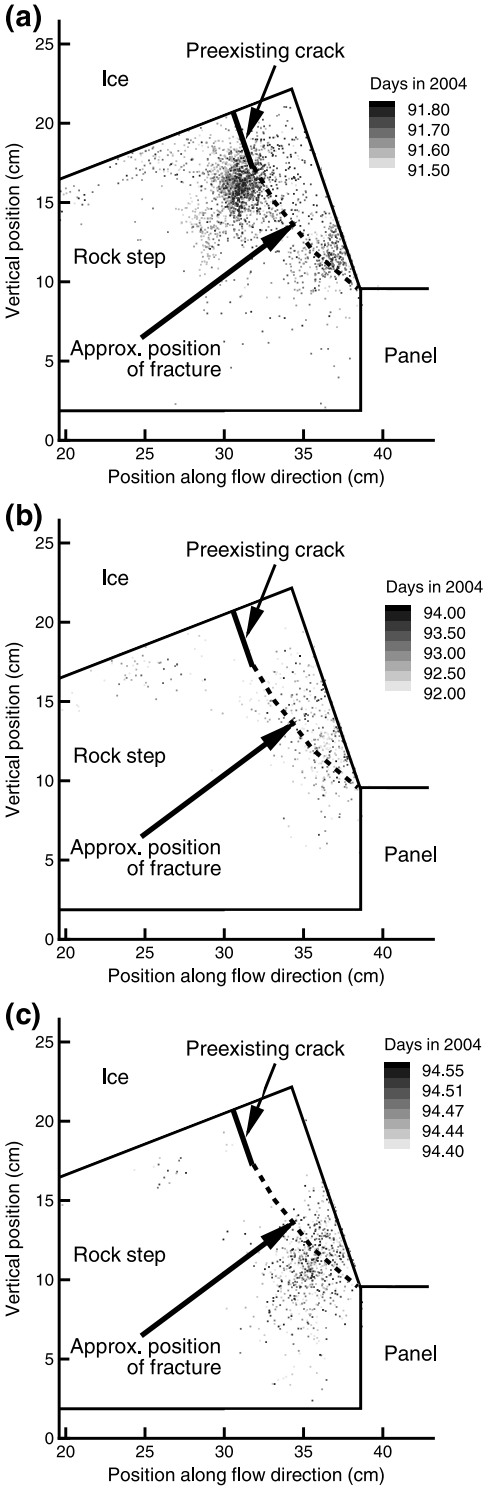

Figure 8. Location of AE events in the plane parallel to ice flow during (a) PT1, (b) between PT1 and PT2, and (c) PT2a,b. Each square indicates an event captured by all eight sensors. Shading indicates timing of event. Outlines of granite step, panel, preexisting crack, and fracture made during the experiment are also shown.

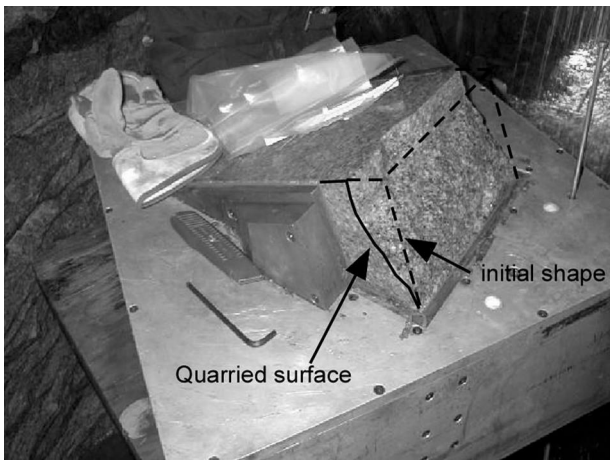

Figure 9. Step at end of experiment with quarried lee surface.

pumping ended, ice began to close progressively on the step, as indicated by the increasing mean stress on it, followed by the abrupt reconnection of the ice with the flat part of the panel upstream about 2.5 hours later.

[35] Results of PT2a and PT2b were quite different because gaps around the panel had become sealed with sediment, so water could not easily drain through the panel into the shaft. As a result, high water pressure was attained rapidly, pumping could be sustained only briefly, and water pressure decayed more slowly after pumping than in PT1 (Figure 6b). Owing to the short pumping duration, ice-bed separation was less than in PT1, with no major reductions in stress on the step or the panel upstream that would indicate ice-bed separation. Also, no ice-bed separation could be detected with the point gauge (Figure 6b), restricting

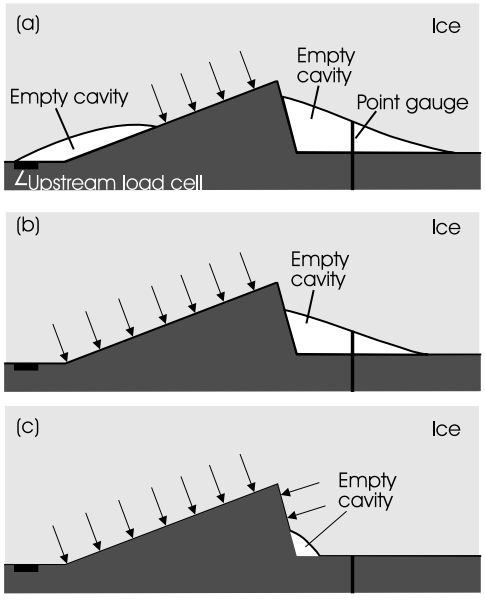

Figure 10. Schematic representations of cavity shape at various stages during PT1. (a) End of pumping, (b) after closure of stoss-side cavity, and (c) during later stage of lee-side cavity closure. Arrows indicate stress that ice or water exerts normal to the step surface.

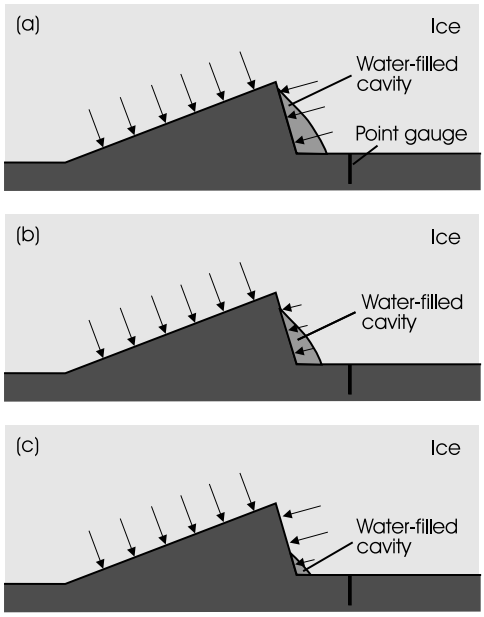

Figure 11. Schematic representations of cavity shape at various stages during PT2a or PT2b. Cavity size was likely larger in PT2b than in PT2a. (a) End of pumping, (b) during initial cavity closure, and (c) during later stage of cavity closure. Arrows indicate normal load of ice or water on step.

possible ice-bed separation to a narrow zone in the lee of the step (Figure 11a). As water pressure fell after pumping, stress on the step and upstream of the step changed but minimally, also consistent with minimal ice-bed separation. The peak in stress upstream of the step that occurred after the water pressure pulses likely reflected the time for the pulse to diffuse through the melt film to the load cell upstream of the step. The two-phase decay in water pressure (Figure 6b) may reflect opening of new hydraulic pathways, such as cracks in the ice or connection with a subglacial drainage system.

[36] Results of PT2c differed from PT2a and PT2b because although the panel remained sealed, a hydraulic pathway along the bed or through the ice enabled sustained pumping with associated high water pressure for more than 1 hour. Point gauge measurements indicated that because of sustained pumping a larger cavity formed in the lee of the step than in PT2a or PT2b, but there was no indication from stresses on the step or panel upstream that there was ice-bed separation elsewhere (Figure 6b). Despite ice-bed separation large enough to be detected with the point gauge, there was little change in stresses on the step or on the panel upstream when pumping was stopped. Perhaps this lack of stress redistribution reflected the slow rate of water pressure decline, which may have allowed creep of ice and resultant cavity closure to occur at rates commensurate with rate of water pressure decline.

6.2. Effects of Stress and Water Pressure on AE Activity

[37] AE activity increased significantly when stresses on the step and on the panel upstream increased (PT1, Figure 6a) or when water pressure in the lee-side cavity dropped rapidly (PT2a and PT2b, Figure 6b). As argued by *Iverson* [1991], reductions in water pressure should cause growth of preexisting cracks by increasing ice pressure against a step's stoss side. The resultant redistribution of stresses on the step's surface increases deviatoric stresses in the rock causing cracks to grow roughly parallel to the most compressive principal stress. Our results agree generally with this argument. After pumping ended in PT1, ice was separated from most of the panel's upper surface including a significant portion of the step (Figure 10a) and water pressure was atmospheric (Figure 6a). As ice closed on the step (Figure 10b), reloading first occurred on the step's stoss side because the smaller stoss-side cavity closed faster than its larger lee-side counterpart and also because sliding of ice ($\sim$12 cm day^{-1} [*Cohen et al.*, 2005]) was faster than the rate of ice closure ($\sim$5 cm day^{-1} for a 10 cm cylindrical cavity, on the basis of earlier measurements beneath Engabreen [*Kohler*, 1993]). This uneven reloading increased deviatoric stresses in the rock resulting in crack growth as indicated by increased AE activity. With continued lee-side ice closure, some ice likely made contact with the step's lee side (Figure 10c). The stress distribution on the step's surface became more uniform, and deviatoric stresses in the rock were reduced resulting in a decrease in AE activity.

[38] In contrast to PT1, the mean stress on the step did not vary significantly during PT2a and PT2b (Figure 6b). Water pressure, however, underwent rapid reductions after pumping ceased. During pumping water under high pressure exerted a normal force on the step's lee side, despite only minimal ice separation (Figure 11a). Because the water pressure was near the mean stress exerted by ice on the step's stoss surface, deviatoric stresses in the rock were minimal. When pumping ceased, water pressure decreased rapidly at a rate faster than ice could creep into the cavity. The normal stress on the step's lee side exerted by water was suddenly reduced (Figure 11b), causing an increase in deviatoric stresses in the rock with resultant increased AE activity (Figure 6b). This interpretation requires that there was minimal hydraulic communication between water in the leeward cavity and water in the crack; otherwise falling water pressure in both the cavity and crack would have caused no change in deviatoric stress at the crack tip. As in PT1, further ice closure on the step's lee side reduced deviatoric stresses in the rock (Figure 11c) causing AE activity to decrease (Figure 6b).

[39] During PT2c (Figure 6b), neither the water pressure nor the mean stress on the step changed rapidly. The rate of cavity closure was likely commensurate with the rate of water pressure decrease, so high deviatoric stresses were not induced in the rock. As a result AE activity did not increase after pumping was stopped. An alternative explanation is that the step was already fully quarried when PT2c was conducted, so there was no large preexisting crack that concentrated stresses at its tip.

[40] Changes in deviatoric stresses in the rock step need not have been large to cause the preexisting crack to grow and AE activity to increase. The highly nonlinear power law relation between crack velocity and stress intensity factor (equation (3)) indicates that minor redistribution of normal stresses caused by water pressure reduction and ice closure can have a large effect on crack velocity.

[41] The position of the crack tip could not be determined precisely from the source locations of AE events (Figure 8) because of their scatter. The migrating center of the locus of AE events indicated, however, that the preexisting crack grew during the experiment along a path that was near the expected orientation of the maximum principal stress (normal to the stoss surface). Few acoustic emissions were recorded between the two pump tests (Figure 8b), perhaps because deviatoric stresses were minimal then and did not exceed the threshold for crack growth or acoustic emissions did not meet the requirement of detection by all eight sensors.

6.3. Effects of Rate of Change of Effective Pressure on AE Activity

[42] Plots of AE activity as a function of the rate of change of effective pressure (Figures 7d–7f) indicate a rough, near-linear correlation after PT1 and PT2a (R^2 = 0.602 and R^2 = 0.434, respectively) but a poor correlation after PT2b (R^2 = 0.0213). After PT1 and PT2a, peaks in AE frequency occurred during rapid increases in effective pressure (Figures 7a and 7b). In contrast, after PT2b the AE frequency peak occurred later, after the effective pressure increase had slowed (Figure 7c), which resulted in the poor correlation. This difference in timing may reflect differences in timescales of cavity closure and effective pressure change. For the illustrative end-member case of no cavity closure, deviatoric stresses in the step and resultant AE activity would increase with the magnitude of the effective pressure, not with its rate of increase. However, if the leeward cavity closes sufficiently rapidly relative to the rate of increase in effective pressure, ice can progressively impinge on and hence support the step's lee surface, thereby reducing deviatoric stresses in the step while effective pressure is still increasing. This effect therefore, which can synchronize rapidly increasing effective pressure with the peak in AE frequency, could be responsible for the apparent correlation between the rate of effective pressure increase and AE activity after PT1 and PT2a. The poor correlation after PT2b may reflect a larger cavity in this case than after PT2a and a resultant longer period required for ice to close on the step's lee surface. A larger cavity following PT2b is expected given the short time that elapsed between it and PT2a. If these interpretations are correct, then correlations between crack growth and effective pressure change are dependent on the many factors that control cavity size and closure rates, so such correlations are expected to be highly variable.

6.4. Effects of Sliding Speed

[43] Although our technique for measuring sliding speed failed, there is little reason to believe the sliding speed was sufficiently variable over the 7-day period to have affected the observed temporal variability in crack growth. As in past pumping experiments beneath Engabreen [*Iverson et al.*, 2003], associated water pressure fluctuations affected only a small area of the bed and therefore should not have caused significant sliding speed variations. Natural variations in sliding velocity were also unlikely; prior measurements beneath Engabreen indicated that in early spring daily changes in sliding speed were small (<10%) [*Cohen et al.*, 2005].

[44] Our measurements do bear, however, on possible reasons why sliding speed may be a good control variable for estimating long-term quarrying rates. High basal water pressure is commonly directly correlated to sliding speed [*Hooke*, 2005], and cavity size also increases with sliding speed [e.g., *Kamb*, 1987]. High basal water pressure optimizes the potential for large reductions in water pressure and associated increases in deviatoric stress in the bed. Large cavities require long periods to close, thereby increasing periods after water pressure reductions when deviatoric stress in the bed is high. Moreover, normal stress increases on stoss surfaces during water pressure reductions are expected to increase in magnitude with the extent of ice-bed separation [e.g., *Iverson*, 1991; *Hallet*, 1996]. These factors leave bedrock bumps and steps beneath glaciers that slide rapidly especially vulnerable to transient basal water pressure and crack growth.

7. Conclusions

[45] To our knowledge, these are the first measurements of crack growth in subglacial rock. They show that a preexisting crack in a granite step grew in response to induced water pressure fluctuations as ice slid past the step. With repeated water pressure fluctuations and resultant changes in ice-bed separation, the crack extended until the step's lee surface was quarried. Results indicate that periods of increasing effective stress, due to either increases in stress on the step's stoss surface or decreasing water pressure on its lee surface, promoted crack growth. Rates of crack growth should also increase significantly during natural fluctuations in water pressure. Long-term quarrying rate may thus be ultimately controlled by the frequency and amplitude of water pressure decreases in lee-side cavities. The magnitude and duration of stress changes on the bed that cause crack growth will increase with cavity size and hence sliding velocity. Future measurements beneath Engabreen will focus on measuring crack growth in a similar step during natural fluctuations in sliding velocity during late spring and summer.

[46] **Acknowledgments.** This project was funded by the U.S. National Science Foundation grant EAR-0229692. We thank John Marchetti and Jon Ljungkull for their contribution to the panel design and Ari Berland for his help in the field. We are grateful to Robert Anderson, Bernard Hallet, and Joseph Walder for their thoughtful reviews.

References

Alley, R. B. (1999), Glacial erosion rates and patterns: Some implications of R. LeB. Hooke's work, *EOS Trans. AGU*, *80*(46), Fall Meet. Suppl. F383.

Alley, R. B., J. C. Strasser, D. E. Lawson, E. V. Evenson, and G. J. Larson (1999), Glaciological and geological implications of basal-ice accretion in overdeepenings, in *Glacial Processes Past and Present*, edited by D. M. Mickelson and J. W. Attig, *Spec. Pap. Geol. Soc. Am.*, *337*, 1–9.

Anderson, R. S., P. Molnar, and M. A. Kessler (2006), Features of glacial valley profiles simply explained, *J. Geophys. Res.*, *111*, F01004, doi:10.1029/2005JF000344.

Archad, J. F. (1953), Contact and rubbing of flat surfaces, *J. Appl. Phys.*, *24*, 981–988.

Atkinson, B. K. (1984), Subcritical crack growth in geological materials, *J. Geophys. Res.*, *89*(B6), 4077–4114.

Bieniawski, Z. T. (1967), Mechanism of brittle fracture of rock, part I: Theory of the fracture process, *Int. J. Rock Mech. Min. Sci.*, *4*, 395–406.

Boulton, G. S. (1974), Processes and patterns of glacial erosion, in *Glacial Geomorphology*, edited by D. R. Coates, pp. 41–87, Allen and Unwin, St. Leonards, N.S.W., Australia.

Boulton, G. S., E. M. Morris, A. A. Armstrong, and A. Thomas (1979), Direct measurement of stress at the base of a glacier, *J. Glaciol.*, *22*(86), 3–24.

Brace, W. F. (1964), Brittle fracture of rocks, in *State of Stress in the Earth's Crust: Proceedings of the International Conference*, edited by W. R. Judd, pp. 110–178, Elsevier, New York.

Braun, J., D. Zwartz, and J. H. Tomkin (1999), A new surfaces processes model combining glacial and fluvial erosion, *Ann. Glaciol.*, *28*, 282–290.

Breckenridge, F. R., T. M. Proctor, N. N. Hsu, S. S. Fick, and D. G. Eitzen (1990), Transient source for acoustic emission work, in *Progress in Acoustic Emission*, edited by K. Yamaguche, H. Takahashi, and H. Niitsuma, pp. 20–37, Jpn. Soc. for Nondestructive Insp., Tokyo.

Brocklehurst, S. H., and K. X. Whipple (2002), Glacial erosion and relief production in the eastern Sierra Nevada, California, *Geomorphology*, *42*, 1–24.

Chang, S.-H., and C.-I. Lee (2004), Estimation of cracking and damage mechanisms in rock under triaxial compression by moment tensor analysis of acoustic emission, *Int. J. Rock Mech. Min. Sci.*, *41*, 1069–1086.

Charles, R. J. (1958), Static fatigue of glass, *J. Appl. Phys.*, *29*, 1549–1560.

Cohen, D., R. LeB. Hooke, N. R. Iverson, and J. Kohler (2000), Sliding of ice past an obstacle at Engabreen, Norway, *J. Glaciol.*, *46*, 599–610.

Cohen, D., N. R. Iverson, T. S. Hooyer, U. H. Fischer, M. Jackson, and P. L. Moore (2005), Debris-bed friction of hard-bedded glaciers, *J. Geophys. Res.*, *110*, F02007, doi:10.1029/2004JF000228.

Drewry, D. (1986), *Glacial Geologic Processes*, Edward Arnold, London.

Eberhardt, E., D. Stead, and B. Simpson (1999), Quantifying progressive pre-peak brittle fracture damage in rock during uniaxial compression, *Int. J. Rock Mech. Min. Sci.*, *36*, 361–380.

Fountain, A. G., and J. S. Walder (1998), Water flow through temperate glaciers, *Rev. Geophys*, *36*, 299–328.

Hallet, B. (1979), A theoretical model of glacier abrasion, *J. Glaciol.*, *23*, 39–50.

Hallet, B. (1996), Glacial quarrying: A simple theoretical model, *Ann. Glaciol.*, *22*, 1–8.

Hallet, B., L. E. Hunter, and J. Bogen (1996), Rates of erosion and sediment evacuation by glaciers: A review of the evidence, *Global Planet. Change*, *12*, 213–235.

Harbor, J. M. (1992), Numerical modeling of the development of U-shaped valleys by glacier erosion, *Geol. Soc. Am. Bull.*, *104*, 1364–1375.

Hildes, D. H. D., G. K. C. Clarke, G. E. Flowers, and S. J. Marshall (2004), Subglacial erosion and englacial sediment transport modelled for North American ice sheets, *Quat. Sci. Rev.*, *23*, 409–430.

Hooke, R. LeB (2005), *Principles of Glacier Mechanics*, Cambridge Univ. Press, New York.

Humphrey, N. F., and C. F. Raymond (1994), Hydrology, erosion and sediment production in a surging glacier: Variagated Glacier, Alaska, 1982–83, *J. Glaciol.*, *40*, 539–552.

Iverson, N. R. (1990), Laboratory simulation of glacial abrasion: Comparison with theory, *J. Glaciol.*, *36*, 304–314.

Iverson, N. R. (1991), Potential effects of subglacial water-pressure fluctuations on quarrying, *J. Glaciol.*, *21*, 559–562.

Iverson, N. R. (2002), Processes of glacial erosion, in *Modern and Past Glacial Environments*, edited by J. Menzies, pp. 131–145, Elsevier, New York.

Iverson, N. R., D. Cohen, T. S. Hooyer, U. H. Fischer, M. Jackson, P. L. Moore, G. Lappegard, and J. Kohler (2003), Effects of basal debris on glacier flow, *Science*, *301*, 81–84.

Jaeger, J. B., B. Hallet, T. Pavlis, J. Sauber, D. Lawson, J. Milliman, R. Powell, S. P. Anderson, and R. S. Anderson (2001), Orogenic and glacial research in pristine southern Alaska, *EOS Trans. AGU*, *82*(19), 213, 216.

Jahns, R. H. (1943), Sheet structure in granites, its origin and use as a measure of glacial erosion in New England, *J. Geol.*, *51*, 71–98.

Kamb, B. (1987), Glacier surge mechanism based on linked cavity configuration of the basal water conduit system, *J. Geophys. Res.*, *92*(B9), 9083–9100.

Kohler, J. (1993), Engabreen subglacial observatory, in *NVE Report 11*, Norw. Water Resour. Energ. Dir., Oslo, Norway.

Labuz, J. F., and J. M. Bridell (1993), Reducing frictional constraint in compression testing through lubrication, *Int. J. Rock Mech. Min. Sci. Geomech. Abstr.*, *30*(4), 451–455.

Lavrov, A. V., and V. L. Shkuratnik (2005), Deformation- and fracture-induced acoustic emission in rocks, *Acoust. Phys.*, *51*, S2–S11, suppl. 1.

Lawn, B. R., and T. R. Wilshaw (1975), *Fracture of Brittle Solids*, Cambridge Univ. Press, New York.

Lockner, D. (1993), The role of acoustic emission in the study of rock fracture, *Int. J. Rock Mech. Sci. Geomech. Abstr.*, *30*, 883–899.

Loso, M. G., R. S. Anderson, and S. P. Anderson (2004), Post-Little Ice Age record of coarse and fine clastic sedimentation in an Alaskan proglacial lake, *Geology*, *32*, 1065–1068, doi:10.1130/G20839.1.

MacGregor, K. R., R. S. Anderson, S. P. Anderson, and E. D. Waddington (2000), Numerical simulations of glacial-valley longitudinal profile evolution, *Geology*, *28*, 1031–1034.

Molnar, P., and P. England (1990), Late Cenozoic uplift of mountain ranges and global climate change: Chicken or egg?, *Nature*, *346*, 29–34.

Nelder, J. A., and R. Mead (1965), A simplex method for function minimization, *Comput. J.*, *7*, 308–311.

Peng, S., and A. M. Johnson (1972), Crack growth and faulting in cylindrical specimens of Chelmsford granite, *Int. J. Rock Mech. Min. Sci.*, *9*, 37–86.

Raymo, M. E., and W. F. Ruddiman (1992), Tectonic forcing of late Cenozoic climate, *Nature*, *359*, 117–122.

Riihimaki, C. A., K. R. MacGregor, R. S. Anderson, S. P. Anderson, and M. G. Loso (2005), Sediment evacuation and glacial erosion rates at a small alpine glacier, *J. Geophys. Res.*, *110*, F03003, doi:10.1029/2004JF000189.

Scholz, C. H. (1987), Wear and gouge formation in brittle faulting, *Geology*, *15*, 493–495.

Shah, K. R., and J. F. Labuz (1995), Damage mechanisms in stressed rock from acoustic emission, *J. Geophys. Res.*, *100*(B8), 15,527–15,539.

Spotila, J. A., J. T. Buscher, A. J. Meigs, and P. W. Reiners (2004), Long-term glacial erosion of active mountain belts: Example of the Chugach–St. Elias Range, Alaska, *Geology*, *32*, 501–504, doi:10.1130/G20343.1.

Tomkin, J. H. (2003), Erosional feedbacks and the oscillation of ice masses, *J. Geophys. Res.*, *108*(B10), 2488, doi:10.1029/2002JB002087.

D. Cohen, N. R. Iverson, and J. F. Thomason, Department of Geological and Atmospheric Sciences, Iowa State University, 253 Science I, Ames, IA 50011, USA. (dcohen@iastate.edu)

T. S. Hooyer, Wisconsin Geological and Natural History Survey, Madison, WI, USA.

M. Jackson, Norwegian Water Resources and Energy Directorate, Oslo, Norway.